PCCP

Accepted Manuscript

ROYAL SOCIETY OF CHEMISTRY

www.rsc.org/pccp

Pulse-coupled BZ oscillators with unequal coupling strengths

Viktor Horvath[†], Daniel J. Kutner[†], John T. Chavis III* and Irving R. Epstein[†]

[†]*Department of Chemistry, Brandeis University, Waltham, MA 02454-9110, USA*

**Center for Applied Math, 657 Rhodes Hall, Cornell University, Ithaca, NY, 14853, USA*

Abstract

Coupled chemical oscillators are usually studied with symmetric coupling, either between identical oscillators or between oscillators whose frequencies differ. Asymmetric connectivity is important in neuroscience, where synaptic strength inequality in neural networks commonly occurs. While the properties of the individual oscillators in some coupled chemical systems may be readily changed, enforcing inequality between the connection strengths in a reciprocal coupling is more challenging. We recently demonstrated a novel way of coupling chemical oscillators, which allows for manipulation of individual connection strengths. Here we study two identical, pulse-coupled Belousov-Zhabotinsky (BZ) oscillators with unequal connection strengths. When the pulse perturbations contain KBr (inhibitor), this system exhibits simple out-of-phase and complex oscillations, oscillatory-suppressed states as well as temporally periodic patterns (N:M) in which the two oscillators exhibit different numbers of peaks per cycle. The N:M patterns emerge due to the long-term effect of the inhibitory pulse-perturbations, a feature that has not been considered in earlier works. Time delay was previously shown to have a profound effect on the system's behaviour when pulse coupling was inhibitory and the coupling strengths were equal. When the coupling is asymmetric, however, delay produces no qualitative change in behaviour, though the 1:2 temporal pattern becomes more robust. Asymmetry in instantaneous excitatory coupling via $AgNO_3$ injection produces a previously unseen temporal pattern (1:N patterns starting with a double peak) with time delay and high [$AgNO_3$]. Numerical simulations of the behaviour agree well with theoretical predictions in asymmetrical pulse-coupled systems.

1. Introduction

Coupling between chemical oscillators has been studied almost as long as periodic behaviour in chemical systems has been the subject of systematic mechanistic investigation [1]. Chemical oscillators may be connected in numerous ways: *e.g.*, diffusively [1-4], electrically [5, 6], using pumps [7-9] or light [10, 11]. When coupling is realised by means of mass transport through a common medium – between two flow reactors connected through an orifice in a common wall [4], or between aqueous droplets suspended in an oil phase [3] – the coupling is necessarily symmetric, because the diffusion rates of the species transferred between two oscillators are equal in both directions.

The overwhelming majority of studies of coupled chemical oscillators employ symmetric coupling [1-4], either between identical oscillators or between oscillators with different frequencies [12]. Asymmetric connectivity is important in neuroscience, where synaptic strength inequality in neural networks is the rule. In fact, plasticity, the modification of synaptic strengths in response to neural activity or environmental changes [13], is the dominant phenomenon in establishing the networks in our brains that facilitate memory and learning [14]. As interest grows in using coupled chemical oscillators as models of neural networks or to perform computations [15-18], it is important to understand the properties of asymmetrically coupled chemical oscillators. While the properties of the individual oscillators in some coupled chemical systems may be easily changed, *e.g.*, by changing input concentrations in a flow reactor (CSTR), enforcing inequality between the connection strengths in a pair of reciprocally coupled oscillators is a more challenging task.

Methods that employ more elaborate instrumentation (*e.g.*, electrical [5] or photochemical [11] coupling) allow for asymmetry in coupling strengths. Asymmetric coupling can also be achieved by connecting two CSTRs of different volumes using peristaltic pumps. In-phase (IP) and anti-phase (AP) oscillations and stabilisation of out-of-phase (OP) oscillations have been reported in such a system [7, 8]. Another example where coupling asymmetry has been realised is the oscillatory electrochemical dissolution of nickel electrodes [19], where anomalous phase synchronisation (synchronisation after initial detuning of oscillators) [20] was

observed: as the coupling strength was increased, the initial frequency heterogeneity of the oscillators first increased slightly. Then, above a critical coupling strength, a rapid transition to complete synchronisation occurred [19, 21]. A number of works that investigate large populations of coupled oscillators suggest that coupling oscillators with identical intrinsic properties (*e.g.*, natural frequencies) is a more tractable problem to study experimentally.

Neural networks may be small (*e.g.*, central pattern generators) [13] or may comprise hundreds to millions of neurons [22]. Synaptic connections may be very different between individual neurons and may, as noted above, undergo dynamical changes during development [23]. The dynamical states that a minimal network of two coupled neurons can produce have been extensively studied [24-31]. Although there are significant differences between neurons and chemical oscillators, their dynamics are governed by the same fundamental principles; therefore observations in coupled chemical systems may shed light on the behaviour of neural systems. Our previous work [32] focused on two pulse-coupled (Belousov-Zhabotinsky) (BZ) oscillators, where the oscillators were identical and the coupling strengths were equal. This system may be viewed as a chemical analogue of two neurons connected through inhibitory or excitatory synapses with spike-mediated neurotransmission. Injections of excitatory or inhibitory species into the BZ system play an analogous role to the release of neurotransmitters in synaptic transmission in neural networks when an action potential reaches the axon terminal. The latency caused by the propagation of action potentials can be emulated in the BZ reaction by means of a delay (τ) between the triggers (peaks of oxidation) and the pulse perturbations. In recent work by Lavrova and Vanag [12], two symmetrically coupled non-identical BZ oscillators were studied using a numerical model. They found that the cycle length ratios of the oscillators determine the behaviour when symmetrical inhibitory and excitatory coupling or mixed (excitatory-inhibitory) coupling is used.

Here we present experimental and numerical results in which the pulse-coupled BZ oscillators are identical, but there is asymmetry *in the coupling strengths*. Our results highlight the importance of the long-term effect of inhibitory perturbations, which may be viewed as an analogue of spike-mediated neuromodulation

[33]. After describing our methods, we report our experimental results, followed by numerical results obtained using a modification of the model used by Lavrova and Vanag [12]. We describe our results with inhibitory coupling in greater length and detail and give only a brief summary of those with excitatory coupling. In this work we do not consider the extreme case where one of the connection strengths goes to zero, which is the periodic forcing studied by many [34-37].

2. Experimental Methods

2.1 Chemicals

Deionised water and the following analytical grade chemicals (without further purification) were used to prepare solutions: $NaBrO_3$ (99+%, Acros Chemicals), tris-(1,10-phenantroline)-iron(II) solution (ferroin) (0.025M, Ricca Chemical Company), malonic acid (MA) (99%, Acros Chemicals), H_2SO_4 (10N, Fisher), KBr (99+%, Janssen Chimica), $AgNO_3$ (100%, Fisher), $HClO_4$ (70%, Fisher), K_2SO_4 (99+%, Acros Chemicals), Triton X-100 (Acros Chemicals).

2.2 Experimental setup

A single pulse-perturbed oscillator was constructed as follows. The reagent feed stocks "A" (containing $NaBrO_3$, H_2SO_4) and "B" (containing MA, ferroin) were continuously pumped into a sealed beaker of volume 15.0 mL using a 4-channel peristaltic pump (Gilson Minipuls 3). The reaction mixture was kept at room temperature and was stirred at rates between 500-800 rpm using a magnetic stirrer (Scinics Instruments, Multistirrer MC 301). Excess reaction mixture exited *via* a PTFE tube through an overflow hole in the top of the reactor. The PTFE tube was connected to a suction flask that was under vacuum generated by an aspirator pump (VAC, Cole Parmer - 75301). Oscillations were followed by monitoring the redox potential (*E*) using a Pt (Radiometer M241PT)-reference (Radiometer REF 321, Ag/AgCl/KCl) electrode pair connected to a pH meter (Oakton pH-510). A glass junction (Radiometer AL-100) filled with saturated K_2SO_4 solution was used to chemically isolate the reaction mixture from the reference electrode and to provide electrical connection between them. The analogue output

of the pH meter was attached to a personal computer via a high precision multichannel data acquisition board (National Instrument NI-6310). The redox potential signal was acquired at a rate of 2 Hz by a custom designed application implemented using LabView [38], which also controlled perturbations through the 5 V digital output channels of the data acquisition board. A reed relay (COTO-9007-00-05-00-1032) was used to toggle the driving potential (12 V) of the solenoid valve (Takasago Japan LTD STV-2-1/4UKG) generated by a precision power supply unit (PSU, Extech 382260). A glass reservoir was mounted on a stand 1.5 m above the reactor and filled with a KBr or $AgNO_3$ perturbing solution. The liquid flow through the PTFE tubes connecting the reservoirs to the reactors was maintained by gravity. Solution levels were kept constant within 5 cm, ensuring a nearly constant flow-rate during each experiment; thus the volume (V_p) of the added perturbing solution was proportional to the time (t_v) for which the solenoid valve remained open. The exact flow rates (around 100 μL/s) were measured daily. The oscillatory cycle length is particularly sensitive to the pH of the reaction mixture; therefore an appropriate amount of H_2SO_4 was added to the KBr perturbing solution and $HClO_4$ to the $AgNO_3$ solution. $HClO_4$ must be used in the presence of silver ion, as SO_4^{2-} at the reagent concentrations would form Ag_2SO_4 precipitate. Concentrations of H_2SO_4 and $HClO_4$ for acidifying the perturbing solutions were calculated so that the $[H^+]$ in the perturbing solution was close to that of the reaction mixtures, typically $[H_2SO_4]$ = 0.25 M, $[HClO_4]$ = 0.325 M. The arrangement is shown in Fig 1.

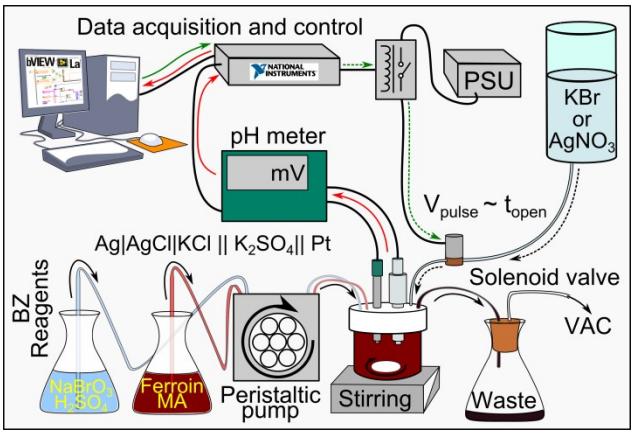

Fig 1 Experimental setup showing a single oscillator. For detailed description and abbreviations, see text in experimental section. Black arrows indicate the flow of reagents and that of the reaction mixture; red and green arrows show data acquisition and control processes, respectively. Dotted lines indicate intermittent flow.

Two physically isolated oscillators were constructed according to the above procedure. Two channels of the 4-channel peristaltic pump supplied the reagents to one oscillator and the other two to the other one. The flow rate ($k_0 = 6.30 \times 10^{-4}$ s^{-1}) of each channel was measured at the beginning of each experimental day and kept around the mean value with a maximum relative deviation of 0.5%. Dedicated monitoring apparatus (electrodes, pH meters), pulse perturbing components (reed relays, solenoid valves, and reservoirs) and excess removal by suction were used to ensure that the oscillators were completely isolated from each other; however, a single recording/processing/controlling unit (PC) was used. The following reagent concentrations were maintained (after dilution and mixing): $[NaBrO_3]_0$ = 0.2 M, $[H_2SO_4]_0$ = 0.25 M, $[MA]_0$ = 0.05 M, $[ferroin]_0 = 1x10^{-3}$ M. We will refer to this composition as "standard." It produces oscillations with a cycle length of about 95 s and amplitude of around 200 mV when uncoupled. Since in this work the amplitude of the oscillations was not considered, normalised redox potential *vs.* time traces are presented.

2.3 Preparations before coupling

We monitored the periods to ensure that they were within the 90-100 s range and were not drifting before turning on the coupling. Fine tuning of the periods was possible by exploiting the sensitivity to the stirring rate. The system was considered to be ready for the experiment when both oscillators maintained target periods for

at least five cycles (around 500 s). The cycle length variation during this time was required to be no more than 5 s. Typically, a lower value was achievable. The relative position of the initial peaks was not controlled, but care was taken that the oscillator that received the stronger coupling would peak first.

2.4 Synapse-like coupling

The coupling scheme was reciprocal (bidirectional) in all experiments: when a high amplitude spike in the redox potential of one oscillator was detected (when the value of *E* crossed a threshold, typically 0.96 V), a pulse perturbation of the other oscillator was triggered. A single pulse had a small volume (typically 10-100 μL) and contained an acidic solution of either the inhibitor (KBr) or the activator ($AgNO_3$). Coupling strength is expressed as the concentration of the added substance ($[KBr]_{inj}$ or $[AgNO_3]_{inj}$) after dilution to the total volume of the reaction mixture.

3. Numerical model

Many models of the BZ oscillator have been proposed, most of which are capable of producing similar dynamics. Although they differ in the number of variables and the level of complexity with which the chemistry is described, the oscillatory dynamics is common to all of them. We chose to extend a recently published numerical model of pulse-coupled BZ oscillators in a flow system by Lavrova and Vanag [12], which we will refer to as the "original" model. Since this model uses only four variables, and the parameters have been adjusted to be comparable to those in experiments similar to our own, we found it a good candidate for performing the large number of calculations necessary to calculate phase diagrams. We also considered other models, but saw no obvious benefit from using a more complex model. The original model is capable of reproducing the experimental results when the coupling is symmetric; it must be extended, however, to reproduce some of the behaviours observed when the coupling is unequal. Therefore we first modified it so that the dynamical features of a single pulse-perturbed BZ oscillator are better reproduced and then extended it to simulate a pair of coupled oscillators. Our primary goal was to suggest reasonably simple modifications that result in good agreement both with the dynamical features of a single BZ oscillator and with those of two pulse-coupled

oscillators. Furthermore, we wanted to employ control parameters (concentrations, flow-rate) comparable with those of our experiments. The chemical feasibility of our proposed modifications is understood to be limited, but a 4-variable model is already an abstraction of the highly complex chemical mechanism of the actual BZ oscillator. Our proposed modifications are based on the experimental observations of a single oscillator discussed in the following sections. These modifications were found to be essential for the model to produce the experimentally observed dynamics when two oscillators are coupled.

3.1 No effect of KBr around the peak

One surprising result with unequal inhibitory coupling is the existence of patterns in which both oscillators spike simultaneously in the absence of time delay. A plausible explanation is that inhibitory pulses have no effect near the peak. To test this hypothesis, we performed experiments in which single perturbations were carried out from 5 s before the peak to 5 s after the peak. These results show that, indeed, the BZ oscillator is insensitive to inhibition in the close vicinity of the peak. When $[KBr]_{inj}$ is 10^{-4} M, its effect is negligible between 1.5 s before a peak and 0.7 s after the peak.

3.2 Long-term effect of inhibitory perturbations

Single pulses do not significantly alter the natural period of the BZ oscillator after the initial cycle in which the pulse is administered: after a single perturbation, recovery of the initial period is almost immediate. However, when perturbations occur over an extended time, the cycle length gradually increases until a plateau is reached. To explore this phenomenon, we performed an experiment in which KBr perturbations were triggered by each peak of a single oscillator (self-coupling). A time delay was necessary, because KBr does not have an inhibitory effect in the immediate vicinity of a peak. A time series of this experiment with $\tau = 30$ s is shown in Fig 2.

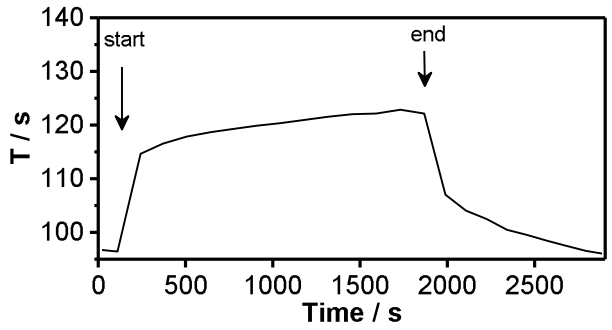

Fig 2 Self-perturbations with 30 s delay. $[KBr]_{inj}$ = 5x10^{-5} M (38 μl), "standard" experimental conditions.

The first perturbation caused a sharp increase in the period of 18 s, about 18% of the initial cycle length. The subsequent perturbations affected the cycle length only moderately: each subsequent cycle was about a second longer than the previous one. This long-term effect reached its maximum after about 10 additional cycles, when the period had increased 26 s from its value at the start of the experiment. These preliminary results suggest that the long-term effect also depends on $[KBr]_{inj}$ and the time since the last peak, but we do not attempt to give a quantitative description of this effect here. When the self-perturbation was interrupted, the natural cycle length was not recovered immediately. There was an initial large drop in the period, in this experiment from 122 s to 107 s, and then the unperturbed period of 98 s was recovered only after 8 more cycles. The recovery time is shorter than can be accounted for by the dilution and replenishment by the inflow; therefore we speculate that the source lies in the complex dynamics rather than a single process. However, further experimental work is required to identify the underlying dynamical and mechanistic reasons for this long-term effect.

3.3 Differential equations of the core BZ model

The following set of differential equations was proposed by Lavrova and Vanag [12] describe the dynamical behaviour of a single unperturbed BZ oscillator in a flow reactor.

$$\frac{dx}{dt} = -k_1 hxy + k_2 h^2 ay - 2k_3 x^2 + k_4 hax\frac{(z_t - z)}{z_t - z + c_{min}} - k_0 x \quad (1)$$

$$\frac{dy}{dt} = -k_1 hxy - k_2 h^2 ay + k_9 vz - k_0 y \quad (2)$$

$$\frac{dz}{dt} = 2k_4hax\frac{(z_t-z)}{z_t-z+c_{min}} - k_9vz - k_{10}bz - k_0z \quad (3)$$

$$\frac{dv}{dt} = 2k_1hxy + k_2h^2ay + k_3x^2 - k_9vz - k_{13}v - k_0v \quad (4)$$

$$c_{min} = \frac{1}{k_{red}}\sqrt{3k_rk_{10}z_t} \quad (5)$$

The variables *x*, *y*, *z* and *v* correspond to the concentrations of the intermediates $HBrO_2$, Br^-, ferriin (oxidised form of the catalyst) and bromo-malonic acid (BrMA). The model parameters were: $k_1 = 2 \times 10^6$ $M^{-2}s^{-1}$, $k_2 = 2$ $M^{-3}s^{-1}$, $k_3 = 3000$ $M^{-1}s^{-1}$, $k_4 = 42$ $M^{-2}s^{-1}$, $k_9 = 20$ $M^{-1}s^{-1}$, $k_{10} = 0.05$ $M^{-1}s^{-1}$, $k_{13} = 5x10^{-3}$ s^{-1}, $c_{min} = (3k_rk_{10}c_0)^{1/2}/k_{red}$, $k_r = 2 \times 10^8$ $M^{-1}s^{-1}$, $k_{red} = 5 \times 10^6$ $M^{-1}s^{-1}$. The concentrations were similar to those used in experiments: $a = [NaBrO_3]_0 = 0.2$ M, $b = [MA] = 0.1$ M, $z_t = [ferroin] = 2$ mM, $h = [H^+] = 0.333$ M, as was the flow rate, $k_0 = 0.00125$ s^{-1}. The unperturbed cycle length was 143.85 s.

Pulse perturbations were triggered when the oxidised catalyst concentration (*z*) reached 90% of the inflow value (z_t) in the model, which occurs around the same time in the cycle when the peak in redox potential occurs in the experiments. The original model employed an extended perturbation window of 5 s, during which *y* was increased with zeroth order kinetics. We have taken a different, but comparable approach: we introduce a variable *p,* which is adjusted instantaneously upon perturbation and decays according to first order kinetics, producing Br^-, which reacts with the intermediates, causing inhibition. Details are given in the Electronic Supplementary Information (ESI).

The extended time window for the effect of an inhibitory pulse is essential in this model. When instantaneous [Br^-] increase was implemented, the pulse-perturbation of a single oscillator did not agree with our experimental observations: the cycles became *shorter* when perturbations occurred close to the peaks, which we did not observe in the experiments. The extended effect is therefore a key component, which ensures that inhibitory perturbations indeed extend the cycle and are ineffective in the vicinity of the peaks. In order to model the long-term effect of perturbations, we also found it necessary to treat the bromate concentration as a variable, as described in the ESI .

To describe experiments in which the oscillators were perturbed with $AgNO_3$, we include, an additional variable, *Ag*, with a flow term and a reaction term that describes the reaction between bromide and silver ions. The differential equation for *y* is augmented by the second order removal of bromide when Ag^+ is present, which is treated as a diffusion controlled reaction ($k_{diff} = 5x10^8\ M^{-1}s^{-1}$).

$$\frac{dAg}{dt} = -k_{diff}yAg - k_0Ag \quad (6)$$

$$\frac{dy}{dt} = -k_1hxy - k_2h^2ay + k_9vz - k_{diff}yAg - k_0y \quad (7)$$

The effect of dilution was included in the model when excitatory perturbations occur, because we found it likely to play a significant role in creating bursting patterns in experiments. When perturbation by $AgNO_3$ occurs, the values of all variables but *Ag* are decreased by 0.66%, which corresponds to the change in concentration in the experiments when a 100 μL perturbation in introduced into the 15 ml reactor volume.

Each oscillator has its own set of differential equations, which were integrated using the ode15s variable order solver for stiff problems included in MATLAB [39]. An absolute tolerance of 10^{-12} and a relative tolerance of 10^{-6} were used. Unless otherwise stated, oscillators 1 and 2 were 29.17 s and 102.08 s into their cycles respectively ($\varphi_{0,1}$ = 0.2, $\varphi_{0,2}$ = 0.7, $\Delta\varphi_0$ = 0.5) at t = 0 s, ensuring that the calculations do not start at a peak and that oscillator 2 peaks first.

4. Experimental results

4.1 Inhibitory coupling (KBr)

With symmetric inhibitory coupling, three distinct types of behaviour were found in previous experiments [32]. At low $[KBr]_{inj}$, the oscillators peaked independently (no synchronisation, NS); anti-phase synchronisation occurred at medium $[KBr]_{inj}$; and when the coupling strength was high, one oscillator oscillated while the other was suppressed (OS). A large class of nonlinear dynamical systems [40-43] display a transition from anti-phase to in-phase oscillations when time delay is introduced. This transition, commonly referred to as phase-flip [44],

occurs in pulse-coupled BZ oscillators as well at medium coupling strengths: almost in-phase synchronisation (AIP) replaced the AP oscillations. In addition to synchronisation, complex temporal patterns (C) were observed when the coupling strength was high and time delay was used.

In these experiments, we varied the concentration of KBr in the pulse-perturbations so that pulses received by oscillator 1 contained lower $[KBr]_{inj}$ than those received by oscillator 2 ($[KBr]_{inj,1} < [KBr]_{inj,2}$). We kept the coupling strengths ($[KBr]_{inj,i}$) constant during the course of each experiment and allowed sufficient time for asymptotically stable states to develop.

When the difference between $[KBr]_{inj,1}$ and $[KBr]_{inj,2}$ was low, we observed out-of-phase oscillations. In order to characterise these, we calculated the phase difference, $\Delta\varphi = (t_2^* - t_1^*)/T_1$, where T_1 is the period of oscillator 1, and t_1^* and t_2^* are the times when consecutive peaks of oscillators 1 and 2 occur, respectively, as shown in Fig 3c.

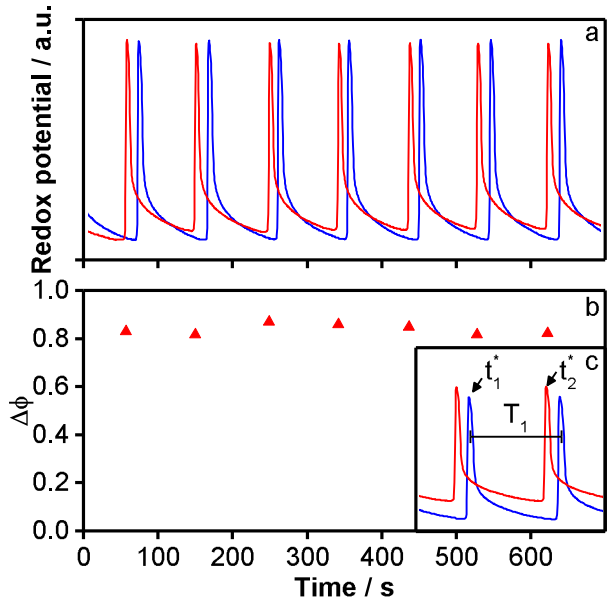

Fig 3 Out-of-phase oscillations with $[KBr]_{inj,1} = 2.5\times10^{-5}$ M, $[KBr]_{inj,2} = 1.83\times10^{-4}$ M, $\tau = 0$s, $\Delta\varphi \approx 0.82$, and "standard" experimental conditions. a) Time series; b) calculated $\Delta\varphi$ values; c) calculation of phase difference $\Delta\varphi$.

Earlier, we observed that, when the coupling is symmetric ($[KBr]_{inj,1}$ = $[KBr]_{inj,2}$), the oscillators synchronise anti-phase ($\Delta\varphi \approx 0.5$). As $[KBr]_{inj,2}$ was increased, a larger phase difference was observed. OP oscillations with a phase difference of approximately 0.82 phase units are shown in Fig 3.

At higher $[KBr]_{inj,2}$ OP synchronisation was replaced by N:M temporal patterns, where N and M refer to the number of peaks of the oscillators within a pattern frame or period ($1 \leq N < M$). We choose the frame boundary at a time when oscillator 2 produces a peak. If a frame contains simultaneous peaks of oscillators 1 and 2, we set the frame boundary there and refer to the pattern as "AF" type (aligned frames); otherwise it is "SF" type (shifted frames). In Fig 4 we show two examples: a 1:2 SF pattern in panel a) and a 2:3 AF pattern in panel b).

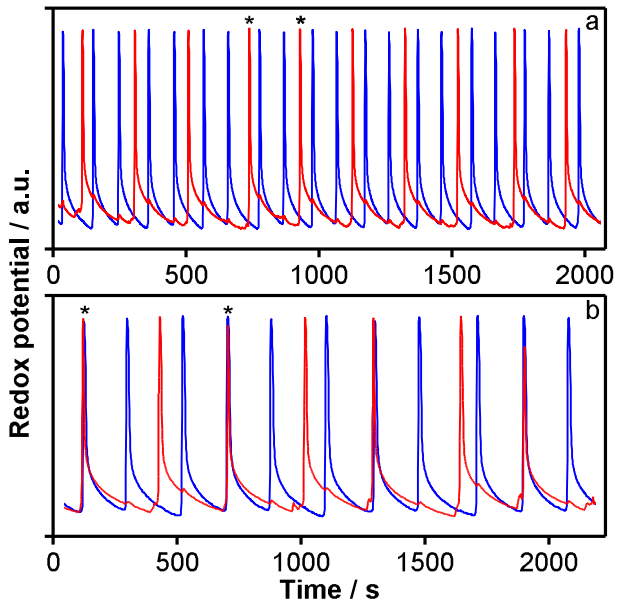

Fig 4 N:M patterns. a) 1:2 SF, $[KBr]_{inj,1} = 3.33x10^{-5}$ M, $[KBr]_{inj,2} = 3.33x10^{-5}$ M, $\tau = 0$ s, b) 2:3 AF, $[KBr]_{inj,1} = 1.67x10^{-5}$ M, $[KBr]_{inj,2} = 1.67x10^{-4}$ M, $\tau = 0$ s. "Standard" experimental conditions. Stars above traces mark peaks defining frame borders.

Although the cycle lengths of oscillators 1 and 2 are nearly equal when uncoupled, the period of oscillator 2 becomes longer than that of oscillator 1 when they are coupled, because $[KBr]_{inj,2}$ is higher and multiple perturbations occur within a cycle of oscillator 2. Cycle lengths of the oscillators display periodic

variation because a) perturbations do not occur in every cycle (1:2 SF pattern, oscillator 1) or b) their position within the cycle varies (2:3 AF pattern, oscillator 1). When we increase $[KBr]_{inj,2}$, other N:M patterns appear in which N = 1 and M > 2, with frames that may or may not contain aligned peaks (Fig 5).

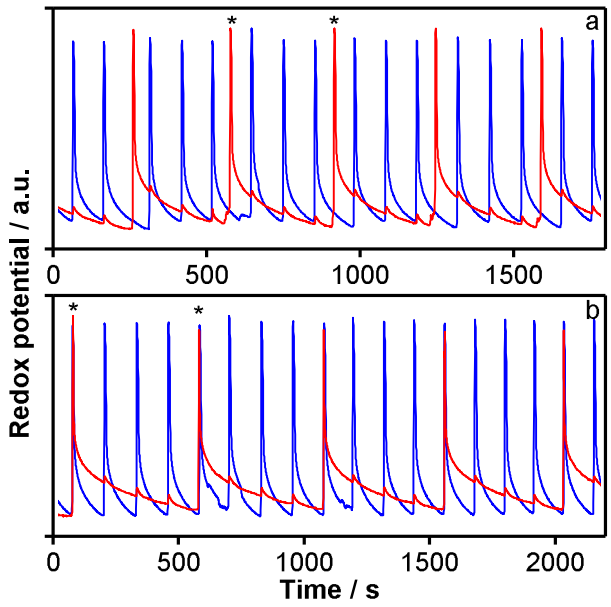

Fig 5 More complex N:M patterns. a) 1:3 SF, $[KBr]_{inj,1} = 3.33x10^{-5}$ M, $[KBr]_{inj,2} = 2.67x10^{-4}$ M, $\tau = 0$ s, b) 1:4 AF, $[KBr]_{inj,1} = 1.67x10^{-5}$ M, $[KBr]_{inj,2} = 3.33x10^{-4}$ M, $\tau = 0$ s, "standard" experimental conditions.

As $[KBr]_{inj,2}$ increases, the ratio N/M diminishes due to the increased inhibition that oscillator 2 experiences in each perturbation. Along with the periodic patterns, we observed some irregular patterns of the 1:N type, in which N varied between 3-7 randomly, as shown in the example in Fig 6a.

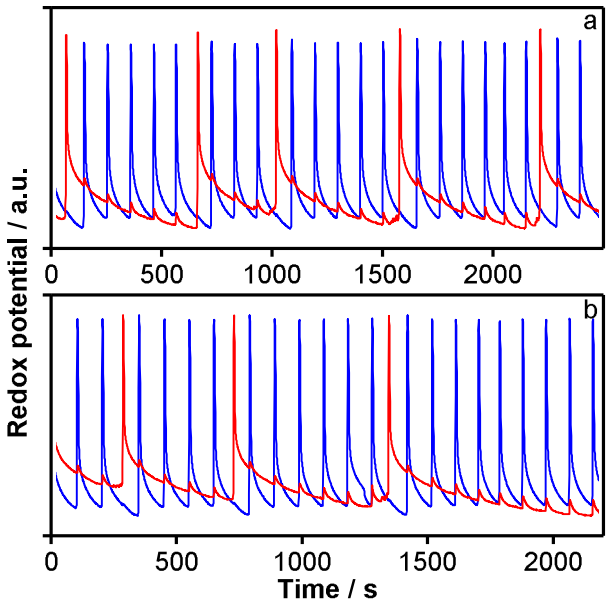

Fig 6 Complex 1:N oscillations. a) Aperiodic variation of N, $[KBr]_{inj,1}$ = 6.67x10^{-5} M, $[KBr]_{inj,1}$ = 3.33x10^{-4} M, τ = 0 s, b) Monotonic increase of N leading to suppression of oscillations, $[KBr]_{inj,1}$ = 3.33x10^{-5} M, $[KBr]_{inj,1}$ = 4.17x10^{-4} M, τ = 0 s, "standard" experimental conditions.

Aperiodic variation of 1:N patterns like that seen in Fig 6a likely occurs because the selected $[KBr]_{inj,1}$ – $[KBr]_{inj,2}$ values are close to the boundaries of two or more 1:N domains, and the experimental noise (small variations of the cycle lengths) causes the system to switch between them. This spontaneous switching between stable domains is similar to that observed in aperiodic mixed-mode oscillations where switching between different stable modes of oscillations occurs due to the existence of a chaotic attractor [45]. However, our experimental data are not sufficient to allow us to confirm the chaotic nature of the observed aperiodic behaviour. We attempt to address this question using our numerical model.

At sufficiently high $[KBr]_{inj,2}$ the inhibition is so strong that oscillator 2 eventually becomes suppressed through a series of 1:N patterns (Fig 6b) where N increases monotonically. We take this kind of pattern to be the low $[KBr]_{inj,2}$ boundary of the oscillatory-suppressed domain. A further increase of $[KBr]_{inj,2}$ shortens the length of the decay into the OS state or causes oscillator 2 to become suppressed immediately while oscillator 1 keeps oscillating at its natural frequency.

The $[KBr]_{inj,1}$–$[KBr]_{inj,2}$ parameter plane summarising our experimental results is shown in Fig 7. The red dashed line indicates symmetric coupling ($[KBr]_{inj,1} = [KBr]_{inj,2}$).

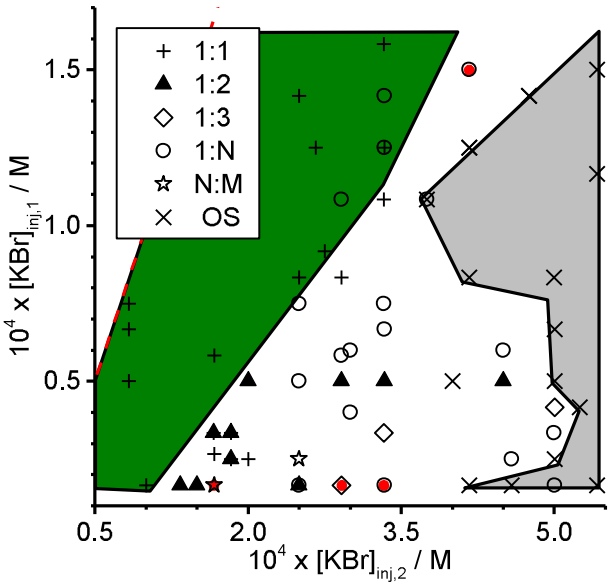

Fig 7 Temporal patterns found in experiments in the $[KBr]_{inj,1}$–$[KBr]_{inj,2}$ parameter plane. Red symbols are AF type patterns; all other patterns are of SF type. (OS: oscillatory-suppressed state.)

The domain of OP oscillations (1:1) is shown in green at the left side of the map, where $[KBr]_{inj,2}$ is low. The boundary of this domain shifts to the right as $[KBr]_{inj,1}$ increases. On the right side of the map, at high $[KBr]_{inj,2}$ the grey domain of OS behaviour is found. The $[KBr]_{inj,2}$ threshold value shows some variation and even decreases as $[KBr]_{inj,1}$ increases between $4x10^{-5}$ and $1x10^{-4}$ M. However, it is problematic to define the exact boundary for each region, as the cycle lengths of the oscillators were not exactly the same in each experiment and the initial phase difference ($\Delta\varphi_0$) was not kept constant.

The N:M patterns are located between the OP and OS domains. Most patterns were of the SF type. The few instances of AF type were seen at lower $[KBr]_{inj,1}$ values. Patterns with aligned peaks are very difficult to observe, because even the slightest variation in the cycle lengths may disrupt them.

When time delay is introduced, patterns predominantly have peaks on their frame boundaries close to aligned ("AF" type). Time delay is an additional dimension and has a significant effect on the behaviour of the system. Short time delays facilitate peak alignment at medium coupling strengths and when the coupling strengths are not very different. The behaviour of the delayed system is predominantly 1:2 AF at medium and low coupling strengths if the coupling asymmetry is not too large. For example, in a system with medium coupling ($[KBr]_{inj,1}$ = 5x10^{-5} M, $[KBr]_{inj,2}$ = 2x10^{-4} M), without delay the initial behaviour is 1:2 SF. When a 10 s time delay is introduced, AIP (1:1) oscillations appear. At a delay of 15 s, 1:2 AF type oscillations arise and persist until the delay reaches 45 s, when the AIP (1:1) oscillations reappear. Since mapping this three-dimensional space is not experimentally feasible, we perform a qualitative assessment of the effect of time delay *via* the numerical simulations described below.

4.2 Excitatory coupling ($AgNO_3$)

When symmetric excitatory coupling was used in our previous work [32], oscillators synchronised in-phase at low and medium coupling strengths ($[AgNO_3]_{inj}$). When the coupling strength was very high, an oscillatory-suppressed state (OS) was observed, in which one oscillator ceased to oscillate, remaining in the oxidised state. This situation differs from the OS state in inhibitory coupling, because there the suppressed oscillator is in the reduced state. When time delay was introduced, in addition to these behaviours, AIP synchronisation (with a phase difference proportional to τ), fast anti-phase (FAP) oscillations with a period around 2τ, and bursting (B) were observed. In the development of FAP oscillations and bursting, we identify time delay, along with the coupling strength, as a key parameter. The transition from AIP oscillations to FAP oscillations is another example of a phase-flip [44].

Not surprisingly, unequal excitatory coupling generates all of the above behaviours when the coupling is close to symmetric. An additional behaviour is seen when $[AgNO_3]_{inj,2}$ is very high: 1:D-N type oscillations ("D" denotes a double peak of oscillator 1), shown in Fig 8.

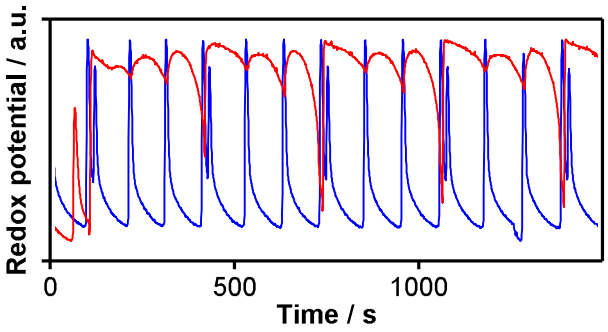

Fig 8 1:D-2 oscillations. $[AgNO_3]_{inj,1}$ = 1.07x10^{-3} M, $[AgNO_3]_{inj,1}$ = 4.00x10^{-5} M, τ = 5 s, "standard" experimental conditions.

Under these experimental conditions (also in the OS regime), $AgNO_3$ no longer functions as an activator from a dynamical point of view. Instead of causing the next cycle to start sooner, the perturbation delays it, because it takes more time for the oscillator to recover from the oxidised state when $AgNO_3$ is present. In a sense, this coupling condition is no longer an excitatory–excitatory situation, but rather of a mixed type, excitatory towards oscillator 1 and inhibitory towards oscillator 2. Previously, we showed that, in a system where one oscillator receives $AgNO_3$ and the other KBr, a host of different 1:N type patterns can develop [32].

A stable 1:D-N pattern requires $[AgNO_3]_{inj,1}$ to be high enough to trigger new peaks immediately. In addition, $[AgNO_3]_{inj,2}$ must be even higher, so that when oscillator 2 receives a perturbation it remains in the oxidised state for a longer time. The following sequence occurs when a stable 1:D-N pattern develops: First, oscillator 1 produces a peak, which is followed by the perturbation of oscillator 2 after the programmed delay. Second, when oscillator 2 transitions to the oxidised state it triggers a countdown to the next perturbation of oscillator 1. When oscillator 1 is next perturbed, oscillator 2 will still be in the oxidised state because $[AgNO_3]_{inj,2}$ is very high. Third, oscillator 1 produces a peak that will cause oscillator 2 to be perturbed (after the delay has elapsed) for the second time in a brief interval. If the amount of $AgNO_3$ received by oscillator 2 is not high enough to keep oscillator 2 from returning to the reduced state before oscillator 1 produces the next peak, then a 1:D-0 ("Double") pattern develops. If the time required for oscillator 2 to return to the reduced state is longer than the next cycle of oscillator 1, another peak of oscillator 1 may occur, which may trigger another

perturbation of oscillator 2, further extending the time it spends in the oxidised state. The more time that passes since the initial double perturbation, the faster oscillator 1 proceeds towards the reduced state. The latter dynamics is brought about by the high $AgNO_3$ excess created when the double perturbation occurs.

When the BZ oscillator is in the oxidised state, oxidation of BrMA occurs, producing bromide ions [46], which gradually turn $AgNO_3$ into AgBr, an inert precipitate. The amount of $AgNO_3$ is much higher than can be precipitated out before the second perturbation in the double perturbation occurs. Since oscillator 2 is still in the oxidised state at the time of the next perturbation, some $AgNO_3$ is still present in the reaction mixture. If this amount combined with the next perturbation is still too high to be eliminated in the form of AgBr before the next perturbation, another perturbation may occur, and the cycle length will be further extended. If the remaining $AgNO_3$ at the time of the latest perturbation is less than that at the time of the previous one, the relaxation to the reduced state will be faster. This can be seen clearly in Fig 8, where the rate of relaxation towards the reduced state of oscillator 2 increases after each perturbation in a 1:D-2 frame.

5. Numerical results

5.1 Inhibitory coupling (KBr)

Asymmetric inhibitory coupling results in five characteristic behaviours: OP synchronisation (1:1), AIP synchronisation (1:1), N:M patterns with or without aligned peaks (N:M SF and N:M AF), and one oscillator active while the other is suppressed (OS). These patterns correspond to those seen in our experiments except for the aperiodic behaviour shown in Fig 6a which we therefore believe is the result of switching between two stable domains due to small variation of cycle lengths in experiments. In Fig 9, we show the simulated $[KBr]_{inj,1}$ *vs* $[KBr]_{inj,2}$ phase planes without delay and with a 30 s delay. The initial phase difference, $\Delta\varphi_0$, is 0.5 in both maps.

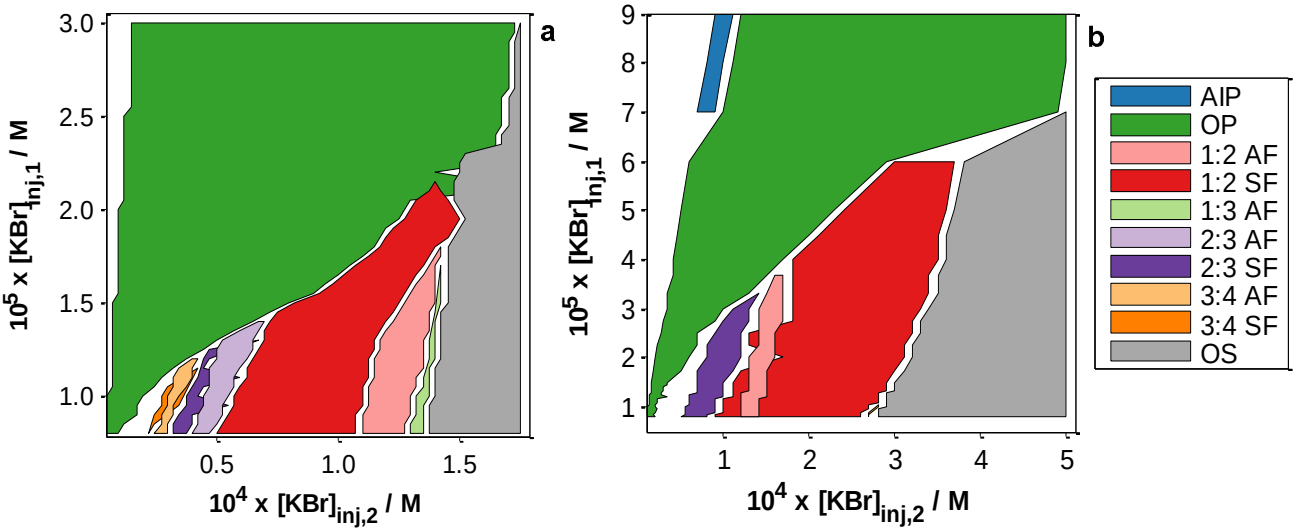

Fig 9 Temporal patterns found in numerical simulations in the $[KBr]_{inj,1}$–$[KBr]_{inj,2}$ phase plane, a) without time delay, b) with 30 s time delay. $\Delta\varphi_0 = 0.5$. Note the difference in the scales. ESI, Fig S1 contains expanded maps showing the full range where both oscillators are active. (AIP: almost in-phase oscillations, OP: out-of-phase oscillations, OS: oscillatory-suppressed state.)

The orientations of the 1:1 OP and OS boundaries are similar to those found experimentally (Fig 7). In the area between these boundaries N:M patterns of both AF and SF type are found. The map shows an arrangement of the temporal patterns domains that is reminiscent of that obtained by Vanag and Epstein [37], where inhibitory periodic forcing of two diffusively coupled oscillators was studied, though here the initial frequencies of the oscillators are equal. Relative to the experiments, the N:M region is shifted to lower $[KBr]_{inj,2}$ and the range in $[KBr]_{inj,1}$ is narrower. The agreement could probably be improved by a) optimizing the parameters so that the periods in numerical simulations (143.85 s) and in experiments (90-100 s) are closer and by b) further work on the long-term effect of repetitive perturbations. Note that the alignment of the peaks occurs regardless of whether time delay is used. Without delay, AF-type patterns are possible only if the oscillators are insensitive to inhibitory perturbations around the peaks. The proportion and the relative positions of the domains in the $[KBr]_{inj,1}$ *vs*. $[KBr]_{inj,2}$ phase diagram strongly depend on the adjustable parameters in our model, which control the insensitivity around the peak. The logarithmic function used to implement the long-

term effect, along with k_{11} (see ESI), determines where the N:M patterns appear, *i.e.*, the boundaries of the 1:1 OP and OS regimes. Rate constants k_{11} and k_{13} determine the main characteristics of the inhibitory effect of the perturbations using KBr. Realistic results may be obtained with values close to those used here. The rate of first order decomposition of BrMA in our model is regulated by k_{13}, which must be within the range $3x10^{-3}$–$5x10^{-3}$ s^{-1}. The corresponding rate term controls the average [BrMA], which in turn regulates the cycle length and the average [Br^-]. If k_{11} is high, addition of KBr causes [BrMA] to increase and thus causes the cycle length to decrease. If, however, k_{11} is low, the effect of KBr is much smaller, and a wider area around the peak will be insensitive to perturbations. Thus the value of k_{11} determines the proportion of AF and SF type N:M patterns. Although, as implemented, the long-term effect is small, it is necessary for the temporally periodic patterns to form. Attempts to reproduce the behaviour with a concentration-independent long-term effect drastically decreased the area of the N:M patterns in the map, a change that we were unable to reverse by adjusting other parameters.

Delay does not result in a significant change in the types of patterns observed (except for the appearance of AIP oscillations at high delay), but it does affect the area of the patterns and the location of the patterns with AF character. The most notable change occurs in the size of the region where both oscillators are active (see Fig S1 in ESI). Without time delay, the upper $[KBr]_{inj}$ limits are $3.5x10^{-4}$ M and $4.5x10^{-4}$ M for oscillators 1 and 2 respectively. When a 30 s time delay is used the window widens, with limits of $[KBr]_{inj,1}$ = $4.5x10^{-4}$ M and $[KBr]_{inj,2}$ = $8x10^{-4}$ M. The domain of 1:2 patterns occupies a greater proportion of the area in which N:M patterns are found, and its structure also changes: the subdomain with AF character shifts from higher $[KBr]_{inj,2}$ to lower values, and at large time delays this domain vanishes entirely (not shown).

The quantitative differences in the phase maps shown in Fig 9 support our observation that time delay is an important control parameter. Therefore, we calculated a phase map where $[KBr]_{inj,1}$ was fixed and τ and $[KBr]_{inj,2}$ varied (Fig 10).

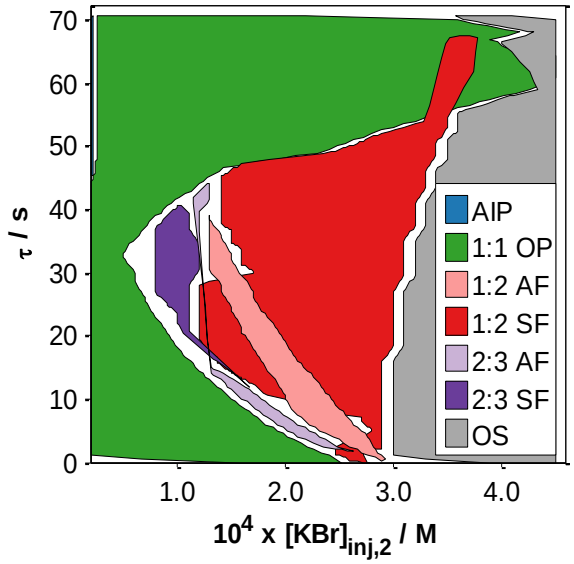

Fig 10 Phase map of behaviours in the $[KBr]_{inj,2}$–τ parameter plane, $[KBr]_{inj,1} = 2x10^{-5}$ M, $\Delta\varphi_0 = 0.5$. (AIP: almost in-phase oscillations, OS: oscillatory-suppressed state.)

The map shows that AIP oscillations only occur in a very narrow strip, as in Fig 9b where $[KBr]_{inj,2}$ is around $2x10^{-5}$ M, *i.e.*, the coupling is nearly symmetric, and where time delays are greater than 45 s. N:M patterns are sandwiched between the domain of OP oscillations and that of OS. 1:2 patterns of the AF and SF type occupy a significant part of the map; above τ = 40 s the subdomain of 1:2 AF type patterns vanishes. The concentration range of N:M patterns is widest when the time delay is about 32 s, approximately 22% of T_0.

Figures 9 and 10 were calculated using a fixed initial phase difference ($\Delta\varphi_0$) of 0.5, where the oscillators are the farthest from each other. We performed additional calculations where we fixed $[KBr]_{inj,1}$, and varied $[KBr]_{inj,2}$, τ and $\Delta\varphi_0$ (see Fig S2 in ESI) in order to examine whether different initial phase differences ($\Delta\varphi_0$) cause the final results to be different. This three-dimensional analysis revealed that the area of the N:M region is largely independent of $\Delta\varphi_0$; only a slight dependence is apparent at low delays close to the OP domain. These results are in qualitative agreement with those of Zeitler *et al.* [30], who looked at pulse-coupled integrate-and-fire models with asymmetrical coupling. The most significant difference is that, in the region of high asymmetry, instead of the marginally stable states found by those authors, we observe asymptotically stable N:M patterns

and the OS regime. These differences can be attributed to the long-term effect of perturbations, which causes non-isochronous behaviour. While the locations of the domains change only slightly as $\Delta\varphi_0$ varies, the alignment of the peaks in the 1:1 domain exhibits dependence on $\Delta\varphi_0$, as shown in Fig 11a.

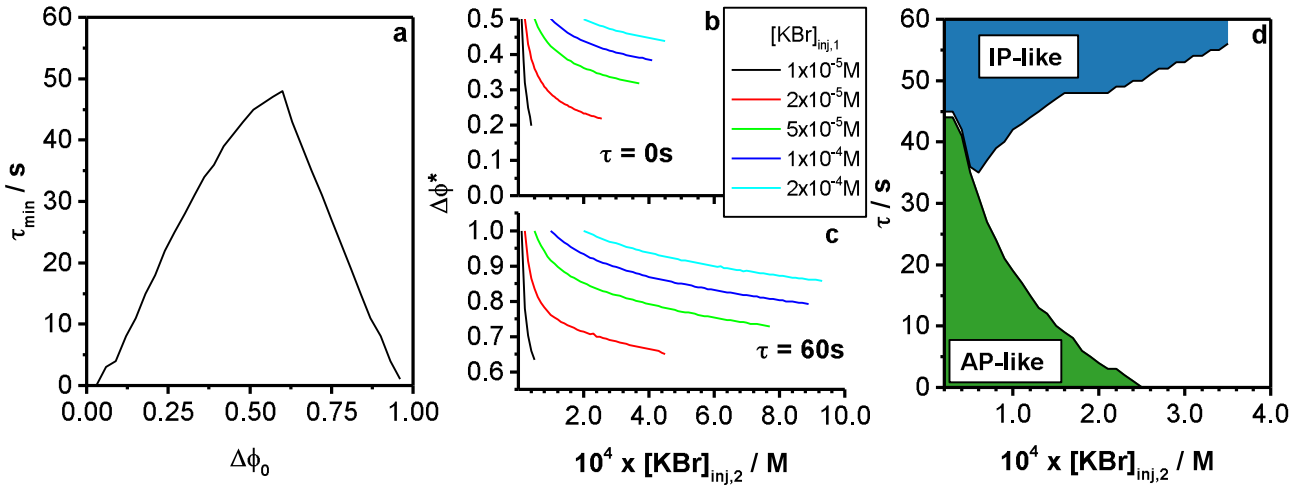

Fig 11 a) Minimum time delay at which AIP oscillations occur as a function of initial phase difference $\Delta\varphi_0$ when $[KBr]_{inj,1} = [KBr]_{inj,2} = 2x10^{-5}$ M. Phase differences of the asymptotically stable states ($\Delta\varphi^*$) as a function of $[KBr]_{inj,2}$ at fixed $[KBr]_{inj,1}$, without time delay (b), and with a 60 s time delay (c). d) Division of the 1:1 domain of Fig 9 into two subdomains of IP-like and AP-like behaviours. (IP: in-phase, AP: anti-phase.)

When the coupling is nearly symmteric, oscillations may occur either anti-phase with an asymtptotically stable final phase arrangement, $\Delta\varphi^*$, of 0.5 or almost in-phase, with $\Delta\varphi^* \approx 0$ (or 1) when time delay is present. When the oscillators are started anti-phase ($\Delta\varphi_0 = 0.5$) a large time delay ($\tau > 48$ s) is required for AIP oscillations to occur. When the simulation is started with the oscillators almost in-phase, the initial phase arrangement is retained. However, without a delay, this AIP arrangement is only metastable: a small fluctuation in cycle length flips the system to the asymptotically stable AP arrangement. In the numerical simulations the cycle length variation is negligible (typically on the order of 10^{-3} s) compared to the window of insensitivity to inhibitory perturbation (roughly 2 s). Therefore AIP oscillations are possible at $\tau = 0$ s if $\Delta\varphi_0 < 0.02$ or $0.98 < \Delta\varphi_0$. However, AIP oscillations do not appear in experiments with $\tau = 0$ s because the naturally occuring cycle length variations are much longer, on the order of a second. As the time delay is increased, the basin of attraction for AP

oscillations shrinks, while that of AIP oscillations grows. For τ between 0 and 48 s, there is a range of bistabiity between the two behaviours.

When the coupling is asymmteric, only OP oscillations occur in the 1:1 domain. While this appears to be a homogeneous domain, the $\Delta\varphi^*$ values depend on $[KBr]_{inj,1}$, $[KBr]_{inj,2}$, and τ (Fig 11b, c). If no time delay is used (Fig 11b), OP oscillations may occur closer to anti-phase: at a fixed $[KBr]_{inj,1}$ $\Delta\varphi^*$ decreases as $[KBr]_{inj,2}$ increases. At higher $[KBr]_{inj,1}$ the minimum of $\Delta\varphi^*$ is higher and the range of $\Delta\varphi^*$ values narrows at a fixed $[KBr]_{inj,1}$. With delay, oscillations may occur close to in-phase (Fig 11c). As $[KBr]_{inj,2}$ increases, so does $\Delta\varphi^*$; at higher $[KBr]_{inj,1}$ the minimum of $\Delta\varphi^*$ is higher. OP oscillations may occur with $\Delta\varphi^* > 0.63$. By comparing the $[KBr]_{inj,2}$ ranges in Fig 11b and c, it is apparent that the 1:1 domain is wider in the presence of time delay. In classifying OP oscillations, we calculate $\Delta\varphi^*$ using the convention that the reference oscillator is oscillator 2, the one that experiences the larger perturbation. These $\Delta\varphi^*$ values can then be assigned as being of AP or IP origin, and thus each OP domain can be divided into two subdomains (Fig 11 d), one containing behaviours related to AP oscillations (with $0.2 > \Delta\varphi^* \geq 0.5$), the other one with those related to IP oscillations (with $0.63 > \Delta\varphi^* \geq 1$).

Variation of $\Delta\varphi^*$ is also observed in the N:M domains. Here we discuss only the 1:2 domain. In the 1:2 pattern oscillator 1 completes two cycles while oscillator 2 completes one. Only one of the cycles of oscillator 1 is affected by a perturbation, resulting in a shorter and a longer cycle. Two phase differences can be calculated for oscillator 1 using the peak of oscillator 2 as reference. In Fig 12 we show the $\Delta\varphi^*$ values as a function of $[KBr]_{inj,2}$ and τ. Traces show the $\Delta\varphi^*$ of the peaks of oscillator 1: blue for the first, red for the second.

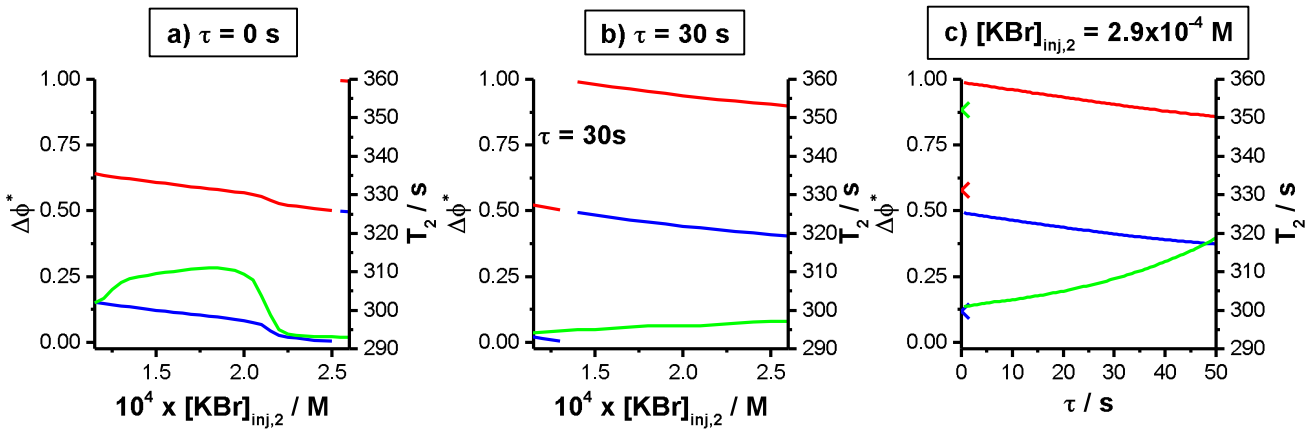

Fig 12 Phase differences at the asymptotically stable states of oscillator 1 in the 1:2 temporal patterns (red = peak 1, blue = peak 2) and period of oscillator 2 (green) as a function of $[KBr]_{inj,2}$ (a, b), and as a function of time delay (c). In a) $\tau = 0$ s, in b) $\tau = 30$ s, in c) $[KBr]_{inj,2} = 2.9 \times 10^{-4}$ M, coloured crosses $\Delta\varphi^*$ at $\tau = 0$ s. In all panels $[KBr]_{inj,1} = 2 \times 10^{-5}$ M, $\Delta\varphi_0 = 0.5$.

When no time delay is used (Fig 12a), at low $[KBr]_{inj,2}$ the two peaks of oscillator 1 occur close to the middle of the cycle of oscillator 2, giving intermediate $\Delta\varphi^*$ values. As $[KBr]_{inj,2}$ increases, the low and high $\Delta\varphi^*$ values decrease, while the difference between the $\Delta\varphi^*$ values for the two peaks remains approximately 0.5, because the first cycle of oscillator 1 in the 1:2 pattern is unperturbed. The period of oscillator 2 increases until it reaches a maximum; it decreases abruptly upon further increase of $[KBr]_{inj,2}$. This rapid change occurs because the second peak of oscillator 1 and the peak of oscillator 2 approach one another as $[KBr]_{inj,2}$ incresaes. Because $\tau = 0$ s and perturbations occuring near a peak are ineffective, the cycle length of oscillator 2 will decrease as the peak of oscillator 2 approaches the insensitive region. At $[KBr]_{inj,2} > 2.5 \times 10^{-4}$ M the peaks of oscillators 1 and 2 switch their order. As a result, a break occurs in the $\Delta\varphi^*$ traces shown in Fig 12 a, while the period of oscillator 2 does not increase further.

With a 30 s delay (Fig 12b) the trends are very similar, but the $\Delta\varphi^*$ values are lower at low $[KBr]_{inj,2}$: the first peak of oscillator 1 and the reference peak of oscillator 2 nearly coincide. As $[KBr]_{inj,2}$ increases, the cycle length of oscillator 2 increases slightly. When $[KBr]_{inj,2}$ reaches 1.4×10^{-4} M, a break occurs in the traces, indicating a switch in the order of the peaks of oscillators 1 and 2.

As shown previously, time delay plays an important role in determining the timing of the peaks in the 1:1 domain. Time delay affects the behaviour in the 1:2 patterns as well: Fig 12c plots the dependence of $\Delta\varphi^*$ on τ at fixed $[KBr]_{inj,1}$ and $[KBr]_{inj,2}$. The traces are discontinuous at $\tau = 0$ s, with the values differing sharply from those with $\tau > 0$ s. Once time delay is introduced, the cycle length of oscillator 2 drops significantly, because the second peak of oscillator 1 now occurs near the peak of oscillator 2 instead of in the middle of its cycle. As the delay increases, the trends are very similar to those seen in Fig 12b: $\Delta\varphi^*$ values decrease, while the difference between the $\Delta\varphi^*$ of peaks 1 and 2 of oscillator 1 remains nearly 0.5. The changes in $\Delta\varphi^*$ can be explained by the cycle length increase of oscillator 2 that are caused by the perturbations occuring later in its cycle as delay increases.

Not surprisingly, when $[KBr]_{inj,1}$ is varied, the opposite trends in $\Delta\varphi^*$ occur (not shown) with only a slight increase in the cycle lengths.

5.1 Excitatory coupling ($AgNO_3$)

An extensive set of simulations, summarised in Fig 13, in the $[AgNO_3]_{inj,1}$–$[AgNO_3]_{inj,2}$ phase plane revealed behaviour similar to that seen in our experiments.

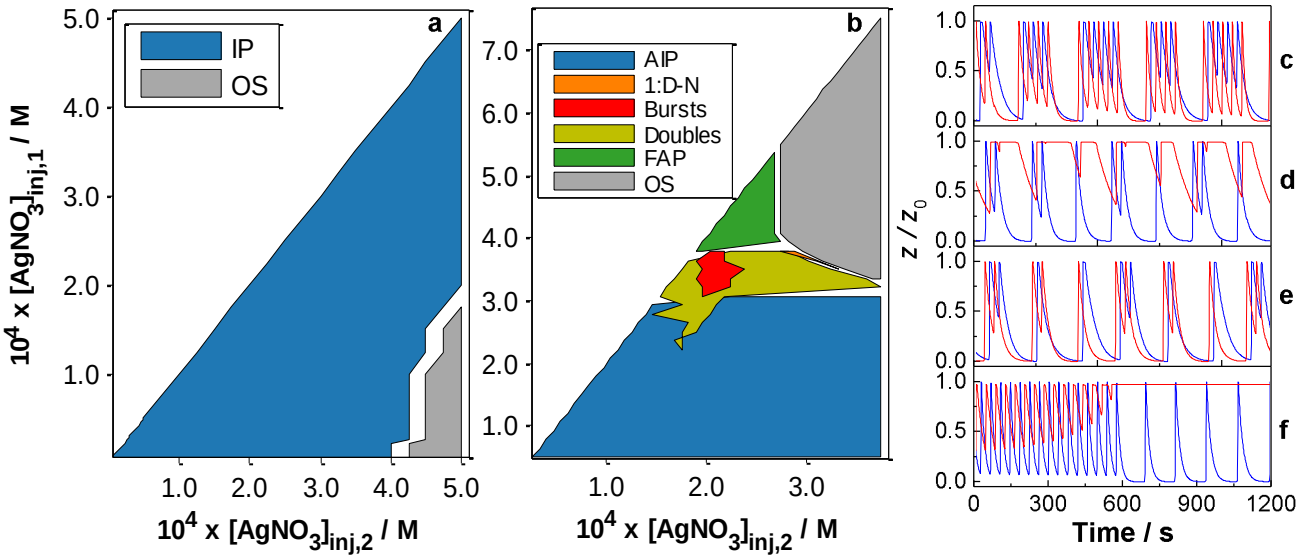

Fig 13 Temporal patterns found in numerical simulations

in the $[AgNO_3]_{inj,1}$–$[AgNO_3]_{inj,2}$ phase plane without time delay (a) and with a 15 s time delay (b). Examples of patterns with τ = 15 s: bursting (c) at $[AgNO_3]_{inj,1} = 3.50\text{x}10^{-4}$ M, $[AgNO_3]_{inj,2} = 3.93\text{x}10^{-4}$ M; 1:D-N (d) at $[AgNO_3]_{inj,1} = 3.79\text{x}10^{-4}$ M, $[AgNO_3]_{inj,2} = 5.79\text{x}10^{-4}$ M; "doubles" (e) at $[AgNO_3]_{inj,1} = 3.24\text{x}10^{-4}$ M, $[AgNO_3]_{inj,2} = 3.64\text{x}10^{-4}$ M; FAP → OS transition (f) at $[AgNO_3]_{inj,1} = 5.21\text{x}10^{-4}$ M, $[AgNO_3]_{inj,2} = 5.50\text{x}10^{-4}$ M. (AIP: almost in-phase oscillations, FAP: fast anti-phase oscillations, OS: oscillatory-suppressed state.)

In the absence of delay (Fig 13a), IP oscillations dominate the phase plane. As the coupling strength is increased, the waveform no longer shows sharp peaks, as the oscillators remain in the oxidised state for some time before returning to the reduced state. Above a threshold of $[AgNO_3]_{inj,2}$, OS emerges due to the accumulation of $AgNO_3$.

When a small time delay (15 s, 0.1 T_0) is used, AIP and FAP oscillations, bursting, and 1:D-N type patterns are seen (Fig 13b). Most of the time series in the domains of "Bursts" and "1:D-N" are not asymptotically stable (a single time series may show several randomly alternating behaviours). We therefore classify each time series based on the most predominant behaviour (occurring more than 50% of the time). Coupling symmetry does not appear to be a strict requirement for bursting patterns to develop. In fact, asymmetry seems to stabilise bursting

with short time delays. Bursting, "doubles" and 1:D-N patterns are quite sensitive to the peak detection threshold value. A low threshold (0.5 z_0) decreases the domain of bursting and almost entirely eliminates 1:D-N.

"Doubles" (Fig 13e) or short bursts contain a double peak in one or both oscillators. This behaviour gives rise to the 1:D-N patterns (Fig 13d), where the "inhibition through activation" becomes strong enough for oscillator 1 to produce multiple peaks while oscillator 2 remains in the oxidised state. These 1:D-N patterns are typically irregular. Short windows with a fixed N may appear, but they tend to show variation in the long term.

Fast anti-phase (FAP) oscillations occur if the coupling is strong enough to trigger a new cycle whenever a perturbation occurs. FAP oscillations may be stable (not shown) or lead to OS when coupling strength is high, as in Fig 13f.

6. Conclusions

We have shown that two pulse-coupled BZ oscillators with asymmetric inhibitory coupling can produce a rich set of temporal patterns. Out-of-phase oscillations with $\Delta\varphi$ other than 0.5 have been detected when coupling strengths are low, which is in agreement with previous experimental work by Yoshimoto *et al.* [7, 8] and Zeitler *et al.* [30]. The N:M patterns constitute a Farey sequence (1:1, 3:4, 2:3, 1:2, 1:3, 1:4, 1:0) as $[KBr]_{inj,2}$ / $[KBr]_{inj,1}$ increases, and they may have aligned peaks on the frame borders of the pattern in the absence of time delay. Similar Farey sequences are found in systems, including the BZ reaction [45,47], that display mixed-mode oscillations [48]. The latter phenomenon, however, typically involves mixtures of small and large amplitude oscillations arising from the existence of multiple time scales in a single oscillator rather than from the coupling of two oscillators with similar time scales.

While patterns with peaks aligned at the frame borders appear as distinct domains in numerical simulations when τ = 0 s, in experiments they are more elusive because the stochastic variation of the period is not negligible. Time delay mainly affects the proportions of the various N:M domains in the $[KBr]_{inj,1}$–$[KBr]_{inj,2}$ phase plane, especially that of the 1:2 temporal pattern, which becomes predominant. The domain of the 1:2

patterns is rather robust when time delay is used, because the delay facilitates tuning the shift between the slow and the fast pulse-trains. While this system produces patterns similar to periodic forcing through activation, these patterns occur due to the stronger inhibition of oscillator 2 rather than due to the cumulative effect of multiple subthreshold excitatory pulses. On the other hand, the temporal patterns are similar to those found with inhibitory periodic forcing (unidirectional coupling), which can be considered as an extreme case of the scenarios studied here where one of the coupling strengths is zero.

Asymmetry in excitatory coupling has a smaller influence on the dynamics of two pulse-coupled BZ oscillators. Without time delay, the effects are practically negligible: in-phase or almost in-phase oscillations were observed both in experiments and numerical simulations. With time delay, we found a new behaviour, 1:D-N type oscillations, at $[AgNO_3]_{inj}$ values where additions of $AgNO_3$ cause the cycle length to increase. Interestingly, bursting patterns with regular spikes seem to be stabilised by coupling asymmetry in this system. Bursting and 1:D-N patterns only occur in a narrow range of time delay (5-18 s). The domain of FAP oscillations increases as τ increases.

Another interesting consequence of asymmetric excitatory coupling is that if the coupling strength difference is large enough, *i.e.*, the larger perturbations received by oscillator 2 produce a much shorter refractory period than that induced by the small perturbations received by oscillator 1, and the delay time is short, a peak order preference arises in the AIP patterns: Oscillator 1 will always peak first, followed soon by oscillator 2. In the preferred arrangement, perturbations to oscillator 1 occur when it is in its refractory state and it therefore fails to peak until its natural time, at which it perturbs oscillator 2, which peaks almost immediately. The other order, in which oscillator 2 peaks first, is unstable. The following two scenarios may occur. If oscillator 1 receives a perturbation when it is in its refractory state it will not produce a peak. When it finally does peak, it will trigger a perturbation to oscillator 2 as described above, and the stable arrangement will appear: oscillator 1 is followed by 2. In the second scenario oscillator 1 receives a perturbation when it is *not* in the refractory state. The resulting peak will trigger a perturbation to oscillator 2 which is *not* in the refractory

period, and it will peak again. The resulting *second* perturbation to oscillator 1 will occur when it is in refractory state, and therefore the first scenario is produced.

Connection asymmetry is common in neural systems: asymmetric excitatory connection has been proposed as the basis of sensing directionality in the retina, and asymmetric inhibitory connections have been shown to enhance retinal selectivity [49]. The long term effect of inhibitory pulses observed in our system is analogous to the adaptation to perturbations reported in certain pacemaker neurons [50]. Synaptic plasticity is widely accepted as the fundamental element of Hopfield associative memory [14]. The strengths of inhibitory connections are also important in the regulation of the dynamics of small neural networks that control signals in certain autonomous rhythmic motor activities like that of the lobster pyloric network [23]. There, activity-dependent modification of inhibitory synapses causes a network of three oscillators to produce dynamical states where various N:M patterns occur before the network settles into a stable physiological behaviour. Mapping the possible dynamical states of asymmetrically coupled oscillatory systems should contribute to a better understanding of how these complex dynamical systems function.

Acknowledgements

This work was supported by the National Science Foundation under grant CHE-1362477 and MRSEC grant DMR-0820492, the Hungarian Academy of Sciences (OTKA K-100891), and the Exceptional Research Opportunities Program (EXROP) of the Howard Hughes Medical Institute (HHMI).

References

1. M. Marek and I. Stuchl, *Biophys. Chem.*, 1975, **3**, 241.
2. M. Dolnik, E. Padusakova and M. Marek, *J. Phys. Chem.*, 1987, **91**, 4407.
3. M. Toiya, V. K. Vanag and I. R. Epstein, *Angew. Chem., Int. Ed.*, 2008, **47**, 7753.
4. M. F. Crowley and I. R. Epstein, *J. Phys. Chem.*, 1989, **93**, 2496.
5. R. Holz and F. W. Schneider, *J. Phys. Chem.*, 1993, **97**, 12239.
6. W. Hohmann, N. Schinor, M. Kraus and F. W. Schneider, *J. Phys. Chem. A*, 1999, 103, 5742.
7. M. Yoshimoto, K. Yoshikawa, Y. Mori and I. Hanazaki, *Chem. Phys. Lett.*, 1992, **189**, 18.
8. M. Yoshimoto, K. Yoshikawa and Y. Mori, *Phys. Rev. E*, 1993, **47**, 864.
9. M. Dolnik and I. R. Epstein, *J. Chem. Phys.*, 1993, **98**. 1149.
10. H. Ke, M. R. Tinsley, A. Steele, F. Wang and K. Showalter, *Phys. Rev*. *E*, 2014, **89**, 052712.
11. S. Nkomo, M. R. Tinsley and K. Showalter, *Phys. Rev. Lett.*, 2013**, 110**, 244102.
12. A. I. Lavrova, V. K. Vanag, *Phys. Chem. Chem. Phys.*, 2014, **16**, 6764.
13. E. Marder and R. L. Calabrese, *Physiol. Rev.*, 1996, **76**, 687.
14. J. J. Hopfield, *PNAS*, 1982, **79**, 2554.
15. A. Adamatzky, B. De L, Costello and T. Asai in *Reaction-Diffusion Computers*, 2005, Elsevier, New York,
16. J. Gorecka and J. Gorecki, *J. Chem. Phys.*, 2006, **124**, 084101.
17. B. de L. Costello, A. Adamtzky, I. Jahan and Liang Zhang, *Chem. Phys.*, 2011, **381**, 88.
18. W. M. Stevens, A. Adamtzky, I. Jahan and B. de L. Costello, *Phys. Rev. E*, 2012, **85**, 066129.
19. M. Wickramasinghe, E. M. Mrugacz and I. Z. Kiss, *Phys. Chem. Chem. Phys.*, 2011, **13**, 15483.
20. B. Blasius, E. Montbrio and J. Kurths, *Phys. Rev. E*, 2003, **67**, 035204(R).
21. B. Blasius, *Phys. Rev. E*, 2005, **72**, 066216.
22. E. R. Kandel in *Principles of Neural Science,* ed. J. H. Schwartz and T. M. Jessell,, 2000, McGraw-Hill, 2nd edn., ch. 2, pt. 1, pp 33-34.
23. C. Soto-Treviño, K. A. Thoroughman, E. Marder and L. F. Abbott, *Nature Neurosci.*, 2001, **4**, 297.

24. C. G. Hocker and I. R. Epstein, *J. Chem. Phys.*, 1989, **90**, 3071.
25. R. E. Mirollo and S. Strogatz, *SIAM J. Appl. Math.*, 1990, **50**, 1645.
26. C. van Vreeswijk, L. F. Abbot and B. Ermentrout, *J. Comp. Neurosci.*, 1994, **1**, 313.
27. U. Ernst, K. Palwelzik and T. Geisel, *Phys. Rev. E.*, 1995, **74**, 1570.
28. U. Ernst, K. Palwelzik and T. Geisel, *Phys. Rev. E.*, 1998, **57**, 2150.
29. P. Goel, B. Ermentrout, *Physica D*, 2002, **163**, 191.
30. M. Zeitler, A. Daffertshofer and C. C. A. M. Gielen, *Phys. Rev. E.*, 2009, **79**, 065203(R).
31. S. Sadeghi and A. Valizadeh, *J. Comp. Neurosci.*, 2014, **36**, 55-66.
32. V. Horvath, P. L. Gentili, V. K. Vanag and I. R. Epstein, *Angew. Chem., Int. Ed.*, 2012, **51**, 6878.
33. S. Zhao, A. F. Sheibanie, M. Oh, P. Rabbah and F. Nadim, *J. Neurosci.*, 2011, **31**, 13991.
34. M. Dolnik, E. Padušáková and M. Marek, *J. Phys. Chem.*, 1987, **91**, 4407.
35. W. Vance and J. Ross, *J. Chem. Phys*. 1989, **91**, 7654.
36. M. Dolnik., I. Berenstein, A. M. Zhabotinsky and I.R. Epstein, *Phys. Rev. Lett*. 2001, **87**, 238301-1-4.
37. V. K. Vanag and I. R. Epstein, *Phys. Rev. E*, 2010, **81**, 06621.
38. LabView 2013 SP1 (32bit), National Instruments Corp., Austin, TX, USA, 2013.
39. MATLAB Release 2014a, The MathWorks, Inc., Natick, MA, USA, 2014.
40. A. Prasad, J. Kurths, S. K. Dana and R. Ramaswamy, *Phys. Rev. E*, 2006, **74**, 035204.
41. A. Prasad, S. K. Dana, R. K. Karnatak, J. Kurths, B. Blasius and R. Ramaswamy, *Chaos*, 2008, **18**, 023111.
42. S. H. Strogatz, *Nature (London)*, 1998, **394**, 316.
43. A. Prasad, *Phys. Rev. E*, 2005, **72**, 056204.
44. A. Sharma, M. D. Shrimali, A. Prasad, R. Ramaswamy and U. Feudel, *Phys. Rev. E*, 2011, **84**, 016226.
45. V. Petrov, S. K. Scott and K. Showalter, *J. Chem. Phys.*, 1992, **97**, 6191.
46. R. J. Field, E. Körös and R. M. Noyes, *J. Am. Chem. Soc.*, 1972, **94**, 8649.
47. R.A. Schmitz, K.R. Graziani and L.L. Hudson, *J. Chem. Phys.,* 1977, **67**, 3040.

48. M. Desroches, J. Guckenheimer, B. Krauskopf, C. Kuehn, H.M. Osinga and M. Wechselberger, *SIAM Rev.,* 2012, **54,** 211**.**

49. A. Koizumi, M. Takavasu and H. Takayasu, *J. Integr. Neurosci.*, 2010, **9**, 337.

50. J. Cui, C. C. Canavier and R. J. Butera, *J. Neurophysiol.*, **102**, 387.